Journal of Sound and Vibration (2002) **250**(5), 773–793
doi:10.1006/jsvi.2001.3960, available online at http://www.idealibrary.com on IDEAL®

A NUMERICAL METHOD FOR SCATTERING FROM ACOUSTICALLY SOFT AND HARD THIN BODIES IN TWO DIMENSIONS

S. A. YANG

Department of Naval Architecture and Marine Engineering, National Cheng Kung University, Tainan, Taiwan, Republic of China. E-mail: yha111@mail.ncku.edu.tw

(*Received* 17 *July* 2000, *and in final form* 7 *March* 2001)

This paper presents a numerical method for predicting the acoustic scattering from two-dimensional (2-D) thin bodies. Both the Dirichlet and Neumann problems are considered. Applying the thin-body formulation leads to the boundary integral equations involving weakly singular and hypersingular kernels. Completely regularizing these kinds of singular kernels is thus the main concern of this paper. The basic subtraction–addition technique is adopted. The purpose of incorporating a parametric representation of the boundary surface with the integral equations is two-fold. The first is to facilitate the numerical implementation for arbitrarily shaped bodies. The second one is to facilitate the expansion of the unknown function into a series of Chebyshev polynomials. Some of the resultant integrals are evaluated by using the Gauss–Chebyshev integration rules after moving the series coefficients to the outside of the integral sign; others are evaluated exactly, including the modified hypersingular integral. The numerical implementation basically includes only two parts, one for evaluating the ordinary integrals and the other for solving a system of algebraic equations. Thus, the current method is highly efficient and accurate because these two solution procedures are easy and straightforward. Numerical calculations consist of the acoustic scattering by flat and curved plates. Comparisons with analytical solutions for flat plates are made.

1. INTRODUCTION

The importance of thin-body scattering problems is well recognized in various physical fields, including acoustics, electromagnetism, and the surface-wave-body interactions [1]. The boundary integral equation method, with appropriate modifications, has been a conventional means of treating this class of problems. Two commonly used approaches are the multi-domain and the thin-body integral formulations. The first [2] introduces an imaginary interface surface that divides the acoustic domain into an interior subdomain and an exterior subdomain. Integral equations for the interior and the exterior subdomains are coupled using continuity conditions at the interface surface. This approach is not efficient in computation if the imaginary interface surface is relatively large. The second approach, proposed by Wu and Wan [3], is conceptually similar to the previous one because an imaginary interface surface is also constructed. This approach considers the integral equation and its normal derivative of each subdomain. By combining the interior and exterior integral equations, Wu and Wan [3] could cancel out the integrals over the imaginary interface surface in terms of the corresponding continuity conditions. The advantage over the multi-domain formulation is that only the integrals over the body

0022-460X/02/100773 + 21 $35.00/0

surface are required. However, this approach introduces another more difficult problem, i.e., the hypersingularity.

Developing a means of efficiently evaluating hypersingular integral equations has become an active research topic in the acoustic radiation and scattering problems since Burton and Miller [4] derived a method of overcoming the non-uniqueness difficulty. This method linearly combines the Helmholtz integral equation with its normal derivative. Schenck [5] proposed the so-called combined Helmholtz integral equation formulation (CHIEF) method that also overcomes the non-uniqueness difficulty. Although Burton and Miller's method possesses a more rigorous mathematical background than the CHIEF method, the hypersingularity difficulty is known to largely hinder the numerical implementation of the composite equation. This fact accounts for why the CHIEF method has been extensively used in engineering applications nowadays. Non-uniqueness occurs at the characteristic frequencies (more precisely, in a frequency band with a certain characteristic frequency as the center) of bodies with finite volume. When the body volume degenerates, non-uniqueness disappears. Under such circumstances, the standard integral formulation fails ascribed to the fact that the opposite surfaces collapse into one; then we can apply the two solution methods mentioned previously. The thin-body formulation can be an effective method if the associated hypersingular integral is easy to evaluate. Wu and Wan [3] adopted Maue's [6] regularized normal derivative integral equation that, however, is not convenient in computation. Other formulations [7–9], derived mainly for the finite body volume, may not be applicable to the thin-body problems. For instance, Yang [9] obtained a set of completely desingularized integral equations using the Gauss flux theorem and other properties of potential theory. Extension of Yang's regularization technology to the thin-body problems fails because some properties of potential theory used are not applicable to thin bodies.

Other related problems include treating mixed boundary conditions; for example, Ih and Lee [10] developed a direct boundary element method so as to evaluate the pressure or the velocity potential on both sides of thin body (with different surface conditions of each side), instead of the jump values across it. Also of interest is the mixed-body condition, i.e., thin bodies (such as fins and wings) mixed with regular bodies (such as the airplane fuselage). Note that the non-uniqueness difficulty mentioned previously still exists in the mixed-body boundary integral formulation so that the use of, for example, the CHIEF method or the Burton–Miller method is required [11].

The purpose of this paper is to develop an efficient solution method of treating 2-D thin-body scattering problems. The thin-body formulation is adopted and briefly described in section 2. Burton and Miller's method is known to lose the advantage over Schenck's method due to the hypersingularity, as mentioned above. We present a means of efficiently evaluating the related hypersingular integral so as to avoid the occurrence of Burton and Miller's difficulty. Sections 3 and 4 describe the desingularization techniques for thin soft and thin rigid bodies. We approximate the unknown function by means of truncated series of Chebyshev polynomials. The Chebyshev polynomials have acquired great practical importance in polynomial approximation method. Specifically, it has been shown that a series of Chebyshev polynomials converges more rapidly than other series of Gegenbauer polynomials, and it converges much more rapidly than a power series. For theory and applications involving the Chebyshev polynomials, see reference [12]. From the properties of expansion of functions in Chebyshev polynomials, several researchers [13–15] have extended the expansion method for solving integral equations. The modified hypersingular integral, interpreted in the Hadamard [16] finite-part sense, involved in section 4 is easy to evaluate owing to the fact that an exact value exists [17]. Section 5 examines the proposed method's effectiveness by solving the acoustic scattering from flat and curved plates.

Comparisons with analytical solutions for flat plates are made. Section 6 concludes this paper.

2. THIN-BODY INTEGRAL FORMULATION

The propagation of acoustic waves through an unbounded homogeneous medium is described by the wave equation

$$\nabla^2 \phi(r, t) = \frac{1}{c^2} \frac{\partial^2 \phi(r, t)}{\partial t^2}, \tag{1}$$

where ∇^2 is the Laplacian operator in two dimensions, ϕ is the velocity potential at a point r at time t, and c is the speed of sound in the medium at the equilibrium state. The velocity potential can be written by summing the two parts as follows:

$$\phi = \phi^{inc} + \phi^s, \tag{2}$$

where ϕ^{inc} is the incident velocity potential and ϕ^s is the scattered velocity potential. For a steady state excitation with a time factor $\exp(-\mathrm{i}\omega t)$, equation (1) reduces to the Helmholtz differential equation in the following form:

$$(\nabla^2 + k^2)\phi = 0, \tag{3}$$

where i is the imaginary unit, ω is the angular frequency, and $k = \omega/c$ is the wave number. The excess acoustic pressure can be written as

$$p = -\rho_0 \frac{\partial \phi}{\partial t} = \mathrm{i}\omega\rho_0 \phi, \tag{4}$$

where ρ_0 denotes the density of the fluid at the equilibrium state. The scattered velocity potential should also satisfy the Sommerfeld radiation condition that can be written in 2-D form as

$$\lim_{r \to \infty} r^{1/2} \left| \frac{\partial \phi^s}{\partial r} - \mathrm{i}k\phi^s \right| = 0. \tag{5}$$

Consider a thin body ∂B exposed to a plane wave in an infinite acoustic medium (Figure 1). The thin-body formulation approach [3] is described below. Assume a smooth, twice-differentiable boundary surface $\partial B + \partial b$; the equivalent integral equation of equation (3) takes the form

$$\frac{\phi_e(P)}{2} = \int_{\partial B + \partial b} \left(\phi_e(Q) \frac{\partial G_k(P, Q)}{\partial n_Q} - G_k(P, Q) \frac{\partial \phi_e(Q)}{\partial n_Q} \right) \mathrm{d}S(Q) + \phi^{inc}(P), \quad P \in \partial B + \partial b, \tag{6}$$

where ϕ_e is the velocity potential in the exterior domain, n_Q is the distance in the direction of the outward normal at the source point $Q \in \partial B + \partial b$, ∂B is the body surface and ∂b is the imaginary surface. The free-space Green function in 2-D form can be expressed as

$$G_k(P, Q) = \frac{\mathrm{i}}{4} H_0^{(1)}(kR), \tag{7}$$

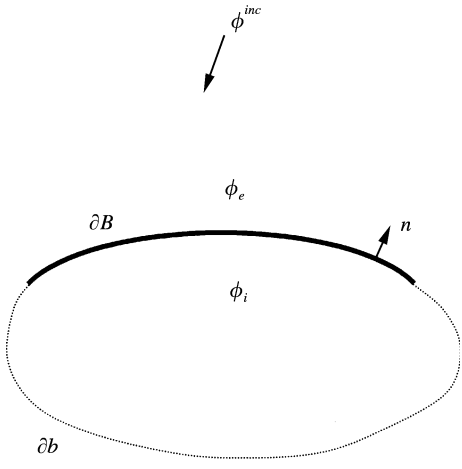

Figure 1. Scattering from a thin body ∂B.

where $H_0^{(1)}(kR)$ denotes the Hankel function of the first kind, R denotes the distance between the field point $P(x, y)$ and the source point $Q(\xi, \eta)$, and (x, y) and (ξ, η) are the corresponding Cartesian co-ordinates. The integral equation for the interior domain is

$$\frac{\phi_i(P)}{2} = \int_{\partial B+\partial b} \left(G_k(P, Q) \frac{\partial \phi_i(Q)}{\partial n_Q} - \phi_i(\mathrm{Q}) \frac{\partial G_k(P, Q)}{\partial n_Q} \right) \mathrm{d}S(Q), \quad P \in \partial B + \partial b, \tag{8}$$

where ϕ_i is the velocity potential in the interior domain. Adding equation (6) and equation (8) together yields

$$\frac{\phi_e(P) + \phi_i(P)}{2} = -\int_{\partial B+\partial b} G_k(P, Q) \left(\frac{\partial \phi_e(Q)}{\partial n_Q} - \frac{\partial \phi_i(Q)}{\partial n_Q} \right) \mathrm{d}S(Q)$$

$$+ \int_{\partial B+\partial b} \frac{\partial G_k(P, Q)}{\partial n_Q} (\phi_e(Q) - \phi_i(Q)) \, \mathrm{d}S(Q) + \phi^{inc}(P). \tag{9}$$

On the imaginary surface ∂b, continuity of the normal component of particle velocity requires

$$\frac{\partial \phi_e}{\partial n} = \frac{\partial \phi_i}{\partial n}, \tag{10}$$

and continuity of pressure requires

$$\phi_e = \phi_i. \tag{11}$$

Applying continuity conditions (10) and (11) in equation (9) leads to

$$\frac{\phi_e(P) + \phi_i(P)}{2} = -\int_{\partial B} G_k(P, Q) \left(\frac{\partial \phi_e(Q)}{\partial n_Q} - \frac{\partial \phi_i(Q)}{\partial n_Q} \right) \mathrm{d}S(Q)$$

$$+ \int_{\partial B} \frac{\partial G_k(P, Q)}{\partial n_Q} (\phi_e(Q) - \phi_i(Q)) \, \mathrm{d}S(Q) + \phi^{inc}(P), \tag{12}$$

where the singular integrals are applied on the body surface ∂B only.

Equation (12) itself is not sufficient for solving the problem ascribed to the additional unknown functions in the interior domain. One more equation is then required to supplement equation (12) for the solution. The normal derivative of equation (9) can be written as

$$\frac{1}{2}\left(\frac{\partial\phi_e(P)}{\partial n_P}+\frac{\partial\phi_i(P)}{\partial n_P}\right)=-\int_{\partial B+\partial b}\frac{\partial G_k(P,Q)}{\partial n_P}\left(\frac{\partial\phi_e(Q)}{\partial n_Q}-\frac{\partial\phi_i(Q)}{\partial n_Q}\right)\mathrm{d}S(Q)$$

$$+\frac{\partial}{\partial n_P}\int_{\partial B+\partial b}\frac{\partial G_k(P,Q)}{\partial n_Q}(\phi_e(Q)-\phi_i(Q))\,\mathrm{d}S(Q)+\frac{\partial\phi^{inc}(P)}{\partial n_P}. \tag{13}$$

Applying continuity conditions (10) and (11) in equation (13) leads to

$$\frac{1}{2}\left(\frac{\partial\phi_e(P)}{\partial n_P}+\frac{\partial\phi_i(P)}{\partial n_P}\right)=-\int_{\partial B}\frac{\partial G_k(P,Q)}{\partial n_P}\left(\frac{\partial\phi_e(Q)}{\partial n_Q}-\frac{\partial\phi_i(Q)}{\partial n_Q}\right)\mathrm{d}S(Q)$$

$$+\frac{\partial}{\partial n_P}\int_{\partial B}\frac{\partial G_k(P,Q)}{\partial n_Q}(\phi_e(Q)-\phi_i(Q))\,\mathrm{d}S(Q)+\frac{\partial\phi^{inc}(P)}{\partial n_P} \tag{14}$$

which contains a hypersingular kernel as $Q\to P$. The derivative $\partial/\partial n_P$ cannot be taken inside the integral since a hypersingular kernel is non-integrable. Equation (14) is actually an integrodifferential equation. Combining equations (12) and (14), however, yields the solution to the problem.

In order to facilitate the numerical implementation, we next express equation (12) and equation (14) in parametric form. Referring to a Cartesian co-ordinate system, the boundary surface ∂B can be represented by a vector function

$$\mathbf{r}(t)=x(t)\mathbf{i}+y(t)\mathbf{j}, \tag{15}$$

where t is an appropriate parameter and $a\leqslant t\leqslant b$. The arc length S of ∂B is given by the integral

$$S(t)=\int_a^t\left(\frac{\mathrm{d}\mathbf{r}(\tau)}{\mathrm{d}\tau}\frac{\mathrm{d}\mathbf{r}(\tau)}{\mathrm{d}\tau}\right)^{1/2}\mathrm{d}\tau, \tag{16}$$

and can also serve as a parameter in parametric representation as follows:

$$\mathbf{r}(S)=x(S)\mathbf{i}+y(S)\mathbf{j}. \tag{17}$$

The ordinary line integral of function $f(x, y)$ along ∂B can then be written by virtue of the parameter t in the following:

$$\int_{\partial B}f(x,y)\,\mathrm{d}S=\int_a^b f(x(t),y(t))\frac{\mathrm{d}S}{\mathrm{d}t}\,\mathrm{d}t, \tag{18}$$

where

$$\frac{\mathrm{d}S}{\mathrm{d}t}=\left(\frac{\mathrm{d}\mathbf{r}}{\mathrm{d}t}\frac{\mathrm{d}\mathbf{r}}{\mathrm{d}t}\right)^{1/2}=\left[\left(\frac{\mathrm{d}x}{\mathrm{d}t}\right)^2+\left(\frac{\mathrm{d}y}{\mathrm{d}t}\right)^2\right]^{1/2}. \tag{19}$$

Note that, in many circumstances, $y(t)$ is not known analytically, but is given by a set of discrete data instead. For the latter case, $y(t)$ can be simulated by using appropriate

approximation methods, for example, a simple cubic spline; section 5 will describe such a numerical application in detail. By following the above discussion and setting $a = -1$ and $b = 1$ in equation (18), we can recast equations (12) and (14) into

$$\frac{f_2(\beta)}{2} = -\int_{-1}^{1} G_k(\beta, \alpha) g_1(\alpha) \frac{\mathrm{d}S}{\mathrm{d}\alpha} \mathrm{d}\alpha + \int_{-1}^{1} \frac{\partial G_k(\beta, \alpha)}{\partial n_\alpha} f_1(\alpha) \frac{\mathrm{d}S}{\mathrm{d}\alpha} \mathrm{d}\alpha + \phi^{inc}(\beta), \tag{20}$$

$$\frac{g_2(\beta)}{2} = -\int_{-1}^{1} \frac{\partial G_k(\beta, \alpha)}{\partial n_\beta} g_1(\alpha) \frac{\mathrm{d}S}{\mathrm{d}\alpha} \mathrm{d}\alpha + \frac{\partial}{\partial n_\beta} \int_{-1}^{1} \frac{\partial G_k(\beta, \alpha)}{\partial n_\alpha} f_1(\alpha) \frac{\mathrm{d}S}{\mathrm{d}\alpha} \mathrm{d}\alpha + \frac{\partial \phi^{inc}(\beta)}{\partial n_\beta}, \tag{21}$$

where α and β are the new parameters corresponding to $Q(\xi, \eta)$ and $P(x, y)$, respectively,

$$f_1 = \phi_e - \phi_i, \tag{22}$$

$$f_2 = \phi_e + \phi_i, \tag{23}$$

$$g_1 = \frac{\partial \phi_e}{\partial n} - \frac{\partial \phi_i}{\partial n}, \tag{24}$$

$$g_2 = \frac{\partial \phi_e}{\partial n} + \frac{\partial \phi_i}{\partial n}, \tag{25}$$

and

$$\frac{\mathrm{d}S}{\mathrm{d}\alpha} = \left[\left(\frac{\mathrm{d}\xi}{\mathrm{d}\alpha} \right)^2 + \left(\frac{\mathrm{d}\eta}{\mathrm{d}\alpha} \right)^2 \right]^{1/2}. \tag{26}$$

Note that the integration limits, -1 and 1, in equations (20) and (21) are purposely selected to facilitate the application of the Chebyshev polynomials to be discussed below.

3. DESINGULARIZATION FORMULATION FOR THE SOFT BODY SCATTERING

For the soft body scattering, i.e., $\phi = 0$ on ∂B, equation (20) reduces to

$$\int_{-1}^{1} G_k(\beta, \alpha) g_1(\alpha) \frac{\mathrm{d}S}{\mathrm{d}\alpha} \mathrm{d}\alpha = \phi^{inc}(\beta). \tag{27}$$

This equation contains a logarithmic type of singularity when $\alpha \to \beta$. We rewrite equation (27) as

$$\int_{-1}^{1} (G_k(\beta, \alpha) - G_0(\beta, \alpha)) g_1(\alpha) \frac{\mathrm{d}S}{\mathrm{d}\alpha} \mathrm{d}\alpha + \int_{-1}^{1} G_0(\beta, \alpha) g_1(\alpha) \frac{\mathrm{d}S}{\mathrm{d}\alpha} \mathrm{d}\alpha = \phi^{inc}(\beta), \tag{28}$$

where G_0 denotes the free-space Green's function for the Laplace equation. A 2-D form of G_0 can be expressed as

$$G_0 = -\frac{\ln R}{2\pi}. \tag{29}$$

The relationship

$$R = [(x-\xi)^2 + (y-\eta)^2]^{1/2}$$

$$\approx \frac{\mathrm{d}S}{\mathrm{d}\beta}|\alpha-\beta|, \text{ as } |\alpha-\beta| \to 0, \tag{30}$$

motivates us to rewrite equation (28) in the following form:

$$\int_{-1}^{1} (G_k(\beta,\alpha) - G_0(\beta,\alpha)) g_1(\alpha) \frac{\mathrm{d}S}{\mathrm{d}\alpha}\mathrm{d}\alpha - \frac{1}{2\pi}\int_{-1}^{1}\left[\ln R - \ln\left(\frac{\mathrm{d}S}{\mathrm{d}\beta}|\alpha-\beta|\right)\right] g_1(\alpha)\frac{\mathrm{d}S}{\mathrm{d}\alpha}\mathrm{d}\alpha$$

$$-\frac{1}{2\pi}\ln\frac{\mathrm{d}S}{\mathrm{d}\beta}\int_{-1}^{1} g_1(\alpha)\frac{\mathrm{d}S}{\mathrm{d}\alpha}\mathrm{d}\alpha - \frac{1}{2\pi}\int_{-1}^{1}\ln|\alpha-\beta| g_1(\alpha)\frac{\mathrm{d}S}{\mathrm{d}\alpha}\mathrm{d}\alpha = \phi^{inc}(\beta). \tag{31}$$

The normal and also the normal derivative at a point on the body's edges cannot be defined; the function $g_1(\alpha)$ is notably proportional to $(1 \mp \alpha)^{-1/2}$ as $\alpha \to \pm 1$ [18]. Note also that the weighting function of the Chebyshev polynomials of the first kind T_n happens to be $(1-\alpha^2)^{-1/2}$. This observation suggests the following expansion:

$$g_1(\alpha)\frac{\mathrm{d}S}{\mathrm{d}\alpha} = (1-\alpha^2)^{-1/2}\sum_{n=0}^{N} a_n T_n(\alpha), \tag{32}$$

where N is finite and the series coefficients $a_0, \ldots, a_N$ are to be determined. Such an implementation ensures that the edge conditions are satisfied for the surface function $g_1(\alpha)$. Substituting equation (32) into equation (31) yields

$$\sum_{n=0}^{N} a_n \int_{-1}^{1} \frac{G_k - G_0}{(1-\alpha^2)^{1/2}} T_n(\alpha)\,\mathrm{d}\alpha - \frac{1}{2\pi}\sum_{n=0}^{N} a_n \int_{-1}^{1} \frac{\ln R - \ln((\mathrm{d}S/\mathrm{d}\beta)|\alpha-\beta|)}{(1-\alpha^2)^{1/2}} T_n(\alpha)\,\mathrm{d}\alpha$$

$$-\frac{1}{2\pi}\ln\frac{\mathrm{d}S}{\mathrm{d}\beta}\sum_{n=0}^{N} a_n \int_{-1}^{1} \frac{1}{(1-\alpha^2)^{1/2}} T_n(\alpha)\,\mathrm{d}\alpha - \frac{1}{2\pi}\sum_{n=0}^{N} a_n \int_{-1}^{1} \frac{\ln|\alpha-\beta|}{(1-\alpha^2)^{1/2}} T_n(\alpha)\,\mathrm{d}\alpha$$

$$= \phi^{inc}(\beta), \tag{33}$$

where Yang [9] obtained

$$\lim_{R\to 0}(G_k - G_0) = -\frac{1}{2\pi}\left(\gamma + \ln\frac{k}{2}\right) + \frac{\mathrm{i}}{4}, \tag{34}$$

γ is Euler's constant given by $\gamma = \lim_{n\to\infty}(\sum_{m=1}^{n}(1/m) - \ln n) = 0{\cdot}577215\ldots$, and, from equation (30),

$$\lim_{R\to 0}\left[\ln R - \ln\left(\frac{\mathrm{d}S}{\mathrm{d}\beta}|\alpha-\beta|\right)\right] = 0. \tag{35}$$

The first and second integrals, with the preceding two identities, of equation (33) are thus regular and can be conveniently evaluated using the Gauss–Chebyshev integration rule of the first kind [19]

$$\int_{-1}^{1} \frac{1}{(1-\alpha^2)^{1/2}} h(\alpha)\,\mathrm{d}\alpha = \frac{\pi}{J}\sum_{j=1}^{J} h(\alpha_j), \tag{36}$$

where $h(\alpha)$ is a function and $\alpha_j = \cos((2j-1)\pi/2J), j = 1, \ldots, J$. The exact value of the third integral of equation (33) is

$$\int_{-1}^{1} \frac{1}{(1-\alpha^2)^{1/2}} T_n(\alpha)\,\mathrm{d}\alpha = \begin{cases} \pi & \text{for } n = 0, \\ 0 & \text{for } n \geqslant 1, \end{cases} \tag{37}$$

which actually is a use of the orthogonal relation of Chebyshev polynomials T_n and T_m

$$\int_{-1}^{1} \frac{1}{(1-\alpha^2)^{1/2}} T_n(\alpha) T_m(\alpha)\,\mathrm{d}\alpha = \begin{cases} (1+\delta_0)\pi/2 & \text{for } m = n, \\ 0 & \text{for } m \neq n, \end{cases} \tag{38}$$

where

$$\delta_0 = \begin{cases} 1 & \text{for } m = n = 0, \\ 0 & \text{for } m = n \neq 0. \end{cases}$$

The fourth integral of equation (33) can also be evaluated exactly in the following:

$$\int_{-1}^{1} \frac{\ln|\alpha-\beta|}{(1-\alpha^2)^{1/2}} T_n(\alpha)\,\mathrm{d}\alpha = \begin{cases} -\pi \ln 2 & \text{for } n = 0, \\ -\dfrac{\pi T_n(\beta)}{n} & \text{for } n \geqslant 1. \end{cases} \tag{39}$$

The case of $n = 0$ in the preceding equation is well known (see, e.g., integral (699) of reference [20]); the case of $n \geqslant 1$ is obtained by using formula (22.13.3) of reference [19],

$$\int_{-1}^{1} \frac{1}{(\alpha-\beta)(1-\alpha^2)^{1/2}} T_n(\alpha)\,\mathrm{d}\alpha = \pi U_{n-1}(\beta), \tag{40}$$

and the relationship between T_n and U_n

$$\frac{\mathrm{d}T_n(\beta)}{\mathrm{d}\beta} = nU_{n-1}(\beta), \tag{41}$$

where U_n is a Chebyshev polynomial of the second kind.

In computations, we locate the collocation points at the positions of the integration points α_j; the series coefficients $a_0, \ldots,$ and a_N are now easy to evaluate by solving a system of algebraic equations from equation (33). The desired function g_1 is then obtained from equation (32).

For the soft-body scattering, equation (21) reduces to

$$\frac{g_2(\beta)}{2} = -\int_{-1}^{1} \frac{\partial G_k}{\partial n_\beta} g_1(\alpha) \frac{\mathrm{d}S}{\mathrm{d}\alpha}\,\mathrm{d}\alpha + \frac{\partial \phi^{inc}}{\partial n_\beta}. \tag{42}$$

We desingularize equation (42) to the following form:

$$\frac{g_2(\beta)}{2} = -\int_{-1}^{1} \left[\frac{\partial G_k}{\partial n_\beta} g_1(\alpha) - \frac{\partial G_0}{\partial n_\alpha} g_1(\beta)\right] \frac{\mathrm{d}S}{\mathrm{d}\alpha}\,\mathrm{d}\alpha - g_1(\beta) \int_{-1}^{1} \frac{\partial G_0}{\partial n_\alpha} \frac{\mathrm{d}S}{\mathrm{d}\alpha}\,\mathrm{d}\alpha + \frac{\partial \phi^{inc}}{\partial n_\beta}, \tag{43}$$

where the first integral is bounded and the integrand can be set equal to zero when $Q \to P$, and Smirnov [21] obtained

$$\lim_{R\to 0} \frac{\partial \ln R}{\partial n_\alpha} = \frac{\xi'\eta'' - \xi''\eta'}{2(\mathrm{d}S/\mathrm{d}\alpha)^3} = \frac{\kappa(\alpha)}{2}, \tag{44}$$

which is equal to half the curvature $\kappa(\alpha)$ of the boundary curve at $\alpha = \beta$. The function g_2, with g_1 given previously, is obtained by evaluating the non-singular integrals in equation (43) in terms of, again, the Gauss–Chebyshev integration rule of the first kind. Combining g_1 and g_2 yields the solutions $\partial\phi_e/\partial n$ and $\partial\phi_i/\partial n$.

4. DESINGULARIZATION FORMULATION FOR THE HARD BODY SCATTERING

For the hard body scattering, i.e., $\partial\phi/\partial n = 0$ on ∂B, equation (21) reduces to

$$\frac{\partial}{\partial n_\beta} \int_{-1}^{1} \frac{\partial G_k}{\partial n_\alpha} f_1(\alpha) \frac{\mathrm{d}S}{\mathrm{d}\alpha} \mathrm{d}\alpha = -\frac{\partial \phi^{inc}}{\partial n_\beta}. \tag{45}$$

We rewrite equation (45) as

$$\oint_{-1}^{1} \frac{\partial^2 G_k}{\partial n_\alpha \partial n_\beta} f_1(\alpha) \frac{\mathrm{d}S}{\mathrm{d}\alpha} \mathrm{d}\alpha = -\frac{\partial \phi^{inc}}{\partial n_\beta}, \tag{46}$$

where the cross on the integral sign indicates that it is interpreted in the Hadamard [16] finite-part sense. Equation (46) can be further written as

$$\int_{-1}^{1} \left[\frac{\partial^2 (G_k - G_0)}{\partial n_\alpha \partial n_\beta} - \frac{k^2 G_0}{2} \right] f_1(\alpha) \frac{\mathrm{d}S}{\mathrm{d}\alpha} \mathrm{d}\alpha + \frac{k^2}{2} \int_{-1}^{1} G_0 f_1(\alpha) \frac{\mathrm{d}S}{\mathrm{d}\alpha} \mathrm{d}\alpha$$

$$+ \oint_{-1}^{1} \frac{\partial^2 G_0}{\partial n_\alpha \partial n_\beta} f_1(\alpha) \frac{\mathrm{d}S}{\mathrm{d}\alpha} \mathrm{d}\alpha = -\frac{\partial \phi^{inc}}{\partial n_\beta}. \tag{47}$$

By combining equations (30) and (44) with the following equation:

$$\frac{\partial^2 \ln R}{\partial n_\alpha \partial n_\beta} = \frac{1}{R} \frac{\partial^2 R}{\partial n_\alpha \partial n_\beta} - \frac{\partial \ln R}{\partial n_\alpha} \frac{\partial \ln R}{\partial n_\beta}$$

$$= -\frac{1}{R^2} + \frac{\mathbf{n}(\beta)\cdot(\mathbf{n}(\beta) - \mathbf{n}(\alpha))}{R^2} - 2 \frac{\partial \ln R}{\partial n_\alpha} \frac{\partial \ln R}{\partial n_\beta}, \tag{48}$$

we obtain

$$\lim_{R\to 0} \left[\frac{\partial^2 \ln R}{\partial n_\alpha \partial n_\beta} + \frac{1}{(\mathrm{d}S/\mathrm{d}\beta)^2 (\alpha - \beta)^2} \right] = \lim_{R\to 0} \frac{\mathbf{n}(\beta)\cdot(\mathbf{n}(\beta) - \mathbf{n}(\alpha))}{R^2} - \frac{\kappa(\alpha)^2}{2}. \tag{49}$$

Note that

$$\lim_{R\to 0} \frac{\mathbf{n}(\beta)\cdot(\mathbf{n}(\beta) - \mathbf{n}(\alpha))}{R^2} = \lim_{R\to 0} \frac{1 - \cos\theta}{R^2} \approx \lim_{R\to 0} \frac{\theta^2}{2R^2} = \frac{\kappa(\alpha)^2}{2}, \tag{50}$$

where θ is the angle between $\mathbf{n}(\alpha)$ and $\mathbf{n}(\beta)$. Substituting equation (50) into equation (49) gives

$$\lim_{R\to 0}\left[\frac{\partial^2 \ln R}{\partial n_\alpha \partial n_\beta}+\frac{1}{(\mathrm{d}S/\mathrm{d}\beta)^2(\alpha-\beta)^2}\right]=0. \tag{51}$$

Equations (30) and (51) motivate us to rewrite equation (47) in the form

$$\begin{aligned}
&\int_{-1}^{1}\left[\frac{\partial^2(G_k-G_0)}{\partial n_\alpha \partial n_\beta}-\frac{k^2 G_0}{2}\right]f_1(\alpha)\frac{\mathrm{d}S}{\mathrm{d}\alpha}\,\mathrm{d}\alpha-\frac{k^2}{4\pi}\int_{-1}^{1}\left[\ln R-\ln\left(\frac{\mathrm{d}S}{\mathrm{d}\beta}|\alpha-\beta|\right)\right]f_1(\alpha)\frac{\mathrm{d}S}{\mathrm{d}\alpha}\mathrm{d}\alpha\\
&-\frac{k^2}{4\pi}\ln\frac{\mathrm{d}S}{\mathrm{d}\beta}\int_{-1}^{1}f_1(\alpha)\frac{\mathrm{d}S}{\mathrm{d}\alpha}\mathrm{d}\alpha-\frac{k^2}{4\pi}\int_{-1}^{1}\ln|\alpha-\beta|f_1(\alpha)\frac{\mathrm{d}S}{\mathrm{d}\alpha}\mathrm{d}\alpha\\
&-\frac{1}{2\pi}\int_{-1}^{1}\left[\frac{\partial^2 \ln R}{\partial n_\alpha \partial n_\beta}+\frac{1}{(\mathrm{d}S/\mathrm{d}\beta)^2(\alpha-\beta)^2}\right]f_1(\alpha)\frac{\mathrm{d}S}{\mathrm{d}\alpha}\mathrm{d}\alpha\\
&+\frac{1}{2\pi(\mathrm{d}S/\mathrm{d}\beta)^2}\,\text{⨍}\!\!\!\!\!\!-\!\!\int_{-1}^{1}\frac{1}{(\alpha-\beta)^2}f_1(\alpha)\frac{\mathrm{d}S}{\mathrm{d}\alpha}\mathrm{d}\alpha=-\frac{\partial\phi^{inc}}{\partial n_\beta}.
\end{aligned} \tag{52}$$

Equation (52) is to be solved subject to $f_1(\pm 1)=0$. The function $f_1(\alpha)$ is notably proportional to $(1\mp\alpha)^{1/2}$ as $\alpha\to\pm 1$ [18]. Note also that the weighting function of the Chebyshev polynomials of the second kind U_n happens to be $(1-\alpha^2)^{1/2}$. This observation suggests the following expansion:

$$f_1(\alpha)\frac{\mathrm{d}S}{\mathrm{d}\alpha}=(1-\alpha^2)^{1/2}\sum_{n=0}^{N}b_n U_n(\alpha), \tag{53}$$

where N is finite and the series coefficients $b_0,\ldots,b_N$ are to be determined. Such an implementation ensures that the edge conditions are satisfied for the surface function $f_1(\alpha)$. Substituting equation (53) into equation (52) gives

$$\begin{aligned}
&\sum_{n=0}^{N}b_n\int_{-1}^{1}\left[\frac{\partial^2(G_k-G_0)}{\partial n_\alpha \partial n_\beta}-\frac{k^2 G_0}{2}\right](1-\alpha^2)^{1/2}U_n(\alpha)\,\mathrm{d}\alpha\\
&-\frac{k^2}{4\pi}\sum_{n=0}^{N}b_n\int_{-1}^{1}\left[\ln R-\ln\left(\frac{\mathrm{d}S}{\mathrm{d}\beta}|\alpha-\beta|\right)\right](1-\alpha^2)^{1/2}U_n(\alpha)\,\mathrm{d}\alpha\\
&-\frac{k^2}{4\pi}\sum_{n=0}^{N}b_n\ln\frac{\mathrm{d}S}{\mathrm{d}\beta}\int_{-1}^{1}(1-\alpha^2)^{1/2}U_n(\alpha)\,\mathrm{d}\alpha\\
&-\frac{k^2}{4\pi}\sum_{n=0}^{N}b_n\int_{-1}^{1}\ln|\alpha-\beta|(1-\alpha^2)^{1/2}U_n(\alpha)\,\mathrm{d}\alpha
\end{aligned}$$

$$-\frac{1}{2\pi}\sum_{n=0}^{N} b_n \int_{-1}^{1}\left[\frac{\partial^2 \ln R}{\partial n_\alpha \partial n_\beta}+\frac{1}{(\mathrm{d}S/\mathrm{d}\beta)^2(\alpha-\beta)^2}\right](1-\alpha^2)^{1/2}U_n(\alpha)\,\mathrm{d}\alpha$$

$$+\frac{1}{2\pi}\sum_{n=0}^{N}\frac{b_n}{(\mathrm{d}S/\mathrm{d}\beta)^2}\ \text{⨍}_{-1}^{1}\frac{(1-\alpha^2)^{1/2}}{(\alpha-\beta)^2}U_n(\alpha)\,\mathrm{d}\alpha=-\frac{\partial\phi^{inc}}{\partial n_\beta}. \tag{54}$$

Yang [9] obtained that, in the first integral,

$$\lim_{R\to 0}\left[\frac{\partial^2(G_k-G_0)}{\partial n_\alpha \partial n_\beta}-\frac{k^2 G_0}{2}\right]=\frac{k^2}{4\pi}\left(\frac{1}{2}-\ln\frac{k}{2}-\gamma\right)+\mathrm{i}\frac{k^2}{8}, \tag{55}$$

where γ is Euler's constant, as defined in section 3. Observe also that, in the second integral, we have

$$\lim_{R\to 0}\left[\ln R-\ln\left(\frac{\mathrm{d}S}{\mathrm{d}\beta}|\alpha-\beta|\right)\right]=0. \tag{35}$$

The exact value of the third integral of equation (54) is

$$\int_{-1}^{1}(1-\alpha^2)^{1/2}U_n(\alpha)\,\mathrm{d}\alpha=\begin{cases}\pi/2 & \text{for } n=0\\ 0 & \text{for } n\geqslant 1\end{cases} \tag{56}$$

which is a direct use of the orthogonal relation of Chebyshev polynomials U_n and U_m

$$\int_{-1}^{1}(1-\alpha^2)^{1/2}U_n(\alpha)U_m(\alpha)\,\mathrm{d}\alpha=\begin{cases}\pi/2 & \text{for } m=n,\\ 0 & \text{for } m\neq n.\end{cases} \tag{57}$$

The fourth integral of equation (54) can be evaluated exactly in the following:

$$\int_{-1}^{1}\ln|\alpha-\beta|(1-\alpha^2)^{1/2}U_n(\alpha)\,\mathrm{d}\alpha=\begin{cases}\dfrac{\pi\beta^2}{2}-\dfrac{\pi}{4}(1+2\ln 2) & \text{for } n=0,\\ \dfrac{\pi}{2}\left[\dfrac{T_{n+2}(\beta)}{n+2}-\dfrac{T_n(\beta)}{n}\right] & \text{for } n\geqslant 1.\end{cases} \tag{58}$$

The case of $n=0$ in the preceding equation is obtained by combining formula (22.13.4) of reference [19],

$$\text{⨍}_{-1}^{1}\frac{(1-\alpha^2)^{1/2}U_n(\alpha)}{\alpha-\beta}\,\mathrm{d}\alpha=-\pi T_{n+1}(\beta), \tag{59}$$

with the known identity

$$\int_{-1}^{1}(1-\alpha^2)^{1/2}\ln\alpha\,\mathrm{d}\alpha=-\pi(1+2\ln 2)/4; \tag{60}$$

the case of $n\geqslant 1$ is obtained by using equations (41), (59), and formula (22.5.8) of reference [19],

$$T_n(\beta)=(U_n(\beta)-U_{n-2}(\beta))/2. \tag{61}$$

The finite-part integral in equation (54) can be defined in terms of a Cauchy principal-value integral by

$$\oint\!\!\!\!\!\!=_{-1}^{1} \frac{h(\alpha)}{(\alpha-\beta)^2}\,\mathrm{d}\alpha = \frac{\mathrm{d}}{\mathrm{d}\beta} \int_{-1}^{1} \frac{h(\alpha)}{\alpha-\beta}\,\mathrm{d}\alpha, \tag{62}$$

where $h(\alpha)$ is a Hölder-continuous function and has a Hölder-continuous derivative; see references [17, 22] for definitions and further information. By combining equation (62) with equation (59), Kaya and Erdogan [17] obtained

$$\oint\!\!\!\!\!\!=_{-1}^{1} \frac{(1-\alpha^2)^{1/2}\,U_n(\alpha)}{(\alpha-\beta)^2}\,\mathrm{d}\alpha = -\pi(n+1)U_n(\beta). \tag{63}$$

The current expansion method, using the Chebyshev polynomial of the second kind, is seen to greatly facilitate the evaluation of the type of hypersingular integral obtained herein. The first, second and fifth integrals in equation (54) are non-singular, as demonstrated above, and can be conveniently computed by using the following Gauss–Chebyshev integration rule of the second kind [19]

$$\int_{-1}^{1} (1-\alpha^2)^{1/2} h(\alpha)\,\mathrm{d}\alpha = \frac{\pi}{J+1} \sum_{j=1}^{J} h(\alpha_j) \sin^2 \frac{j\pi}{J+1}, \tag{64}$$

where $\alpha_j = \cos(j\pi/(J+1)), j = 1, \ldots, J$.

In computations, we locate again the collocation points at the positions of the integration points x_j; the series coefficients $b_0, \ldots,$ and b_N can thus be determined by solving a system of algebraic equations from equation (54). The desired function f_1 is then obtained from equation (53).

For the hard body scattering, equation (20) reduces to

$$\frac{f_2(\beta)}{2} = \int_{-1}^{1} \frac{\partial G_k}{\partial n_\alpha} f_1(\alpha) \frac{\mathrm{d}S}{\mathrm{d}\alpha}\,\mathrm{d}\alpha + \phi^{inc}(\beta). \tag{65}$$

We desingularize the preceding equation to the following form:

$$\frac{f_2(\beta)}{2} = \int_{-1}^{1} \left[\frac{\partial G_k}{\partial n_\alpha} f_1(\alpha) - \frac{\partial G_0}{\partial n_\beta} f_1(\beta)\right] \frac{\mathrm{d}S}{\mathrm{d}\alpha}\,\mathrm{d}\alpha - \frac{f_1(\beta)}{2\pi} \int_{-1}^{1} \frac{\partial \ln R}{\partial n_\beta} \frac{\mathrm{d}S}{\mathrm{d}\alpha}\,\mathrm{d}\alpha + \phi^{inc}(\beta), \tag{66}$$

where the first integral is bounded and the integrand can be set equal to zero when $Q \to P$, and $\lim_{R\to 0}(\partial \ln R/\partial n_\beta)$ is also bounded, as given in equation (44). The function f_2, with f_1 given previously, is obtained by evaluating the non-singular integrals in equation (66) in terms of, again, the Gauss–Chebyshev integration rule of the second kind. Combining f_1 with f_2 yields the solutions ϕ_e and ϕ_i.

5. NUMERICAL EXAMPLES

This section examines the availability of the soft- and hard-body formulations presented in sections 3 and 4. First, consider an acoustically soft flat plate of width $2d$ exposed to a plane wave at broadside incidence. In this case, the boundary surface is represented by $x = d\alpha$ and $y = \beta = 0$ with $-1 \leqslant \alpha \leqslant 1$ and the transformation function is simply

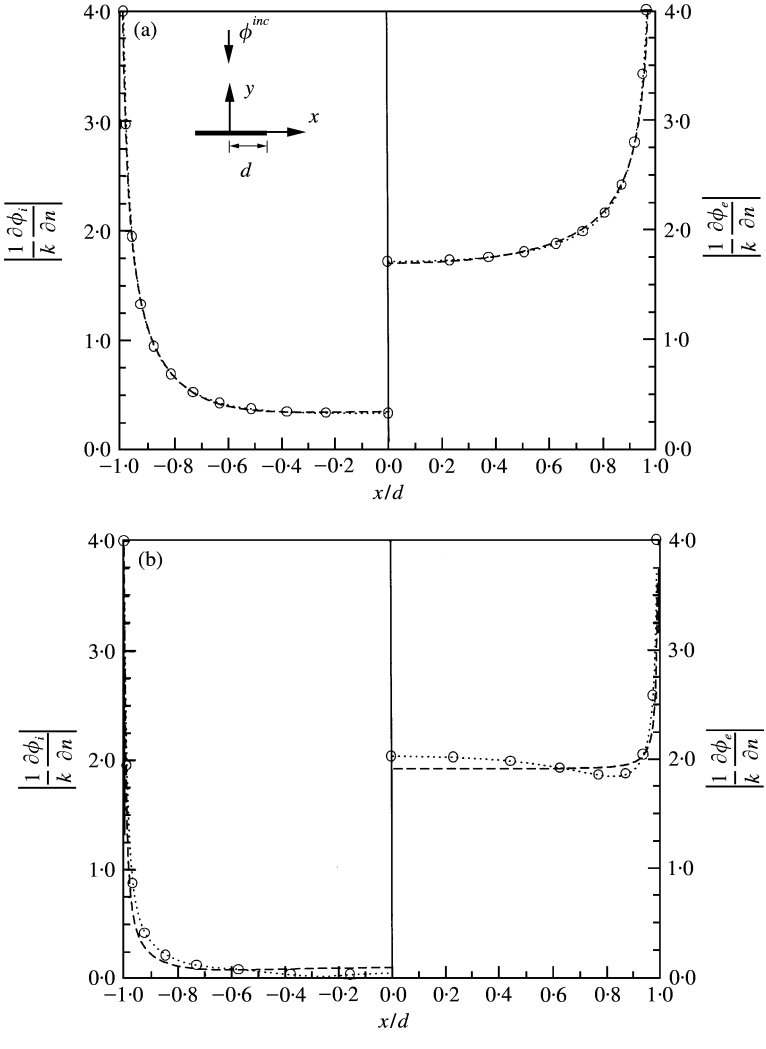

Figure 2. Amplitude of surface field for a soft flat plate exposed to a plane wave with (a) $kd = 1$ and (b) $kd = 5$: ○○○, exact solution; ·····, $N = 10$; – – –, $N = 5$.

$\mathrm{d}S/\mathrm{d}\alpha = d$; the parametric forms (33) and (43) can therefore be easily implemented by the transformation $x = d\alpha$ and $y = \beta = 0$. Figure 2 plots the computed amplitudes of the non-dimensional surface function $k^{-1}\partial\phi/\partial n$ for the cases of $kd = 1$ and 5, and $N = 5$ and 10; this implies that 6 and 11 expansion terms are considered, respectively, for the approximation. The subscript i designates the lower face and e designates the upper face, i.e., the left part of Figure 2 plots the surface function of the lower face and the right part plots that of the upper face. The corresponding exact solution of the surface function is also plotted and can be written as [23]

$$\frac{1}{k}\frac{\partial\phi}{\partial n} = \frac{1}{\upsilon}\left(\frac{8\pi}{1-\tau^2}\right)^{1/2}\sum_{n=0}^{\infty}(-1)^n\left[\frac{Se_{2n}(\upsilon,0)Se_{2n}(\upsilon,\tau)}{N_{2n}^{(e)}Re_{2n}^{(3)}(\upsilon,1)} - \mathrm{i}\frac{So_{2n+1}(\upsilon,0)Se_{2n+1}(\upsilon,\tau)}{N_{2n+1}^{(e)}Ro_{2n+1}^{(3)}(\upsilon,1)}\right], \quad (67)$$

where $\upsilon = kd$, $\tau = \cos\upsilon$, $0 \leqslant \upsilon < 2\pi$, Se and So are the Mathieu even and odd angular functions, respectively, $Re^{(3)}$ and $Ro^{(3)}$ are the Mathieu even and odd radial functions of the

third kind, respectively, and $N_i^{(e)}$ and $N_i^{(o)}$ are defined by the following orthogonal relations:

$$\int_0^{2\pi} Se_i(\upsilon, \cos\upsilon) Se_j(\upsilon, \cos\upsilon)\,\mathrm{d}\upsilon = \begin{cases} 0 & \text{for } i \neq j, \\ N_i^{(e)} & \text{for } i = j, \end{cases} \tag{68}$$

$$\int_0^{2\pi} So_i(\upsilon, \cos\upsilon) So_j(\upsilon, \cos\upsilon)\,\mathrm{d}\upsilon = \begin{cases} 0 & \text{for } i \neq j, \\ N_i^{(o)} & \text{for } i = j, \end{cases} \tag{69}$$

and

$$\int_0^{2\pi} Se_i(\upsilon, \cos\upsilon) So_j(\upsilon, \cos\upsilon)\,\mathrm{d}\upsilon = 0, \tag{70}$$

the last for $i = j$ as well as $i \neq j$; see reference [24] for definitions and further information on Mathieu functions. Figure 2 indicates that the numerical result of $N = 5$ agrees well with the exact solution for the case of $kd = 1$. The numerical results of $N = 10$ for the cases of $kd = 1$ and 5 are extremely close to the exact solutions, as Figure 2 shows. Figure 3 displays the corresponding relative errors ε, defined by |(computed result − exact solution)/exact solution|, of Figure 2 so as to clearly examine the accuracy of the current method. The result of $N = 20$ is also plotted for demonstrating the improvement of accuracy with respect to an increase in the expansion number N. Figure 3 indicates that the relative error of $N = 20$ is $< 10^{-2}$, even very close to the plate's edges where the surface function notably approaches infinity. The relation between the truncation order and the relative error demonstrated in Figure 3 shows that doubling the expansion number N generally improves an order of 10^{-1} in the relative accuracy for both testing wave numbers $kd = 1$ and 5. The computational time took about four times more; this indicates that construction of the matrix elements occupies the major portion of the computational time for the current small-scale problem. Figures 2 and 3 thus confirm the effectiveness of the transformed formulation presented in section 3.

Consider next an acoustically hard flat plate, again, exposed to a plane wave at broadside incidence. The modified formulations (54) and (66) are to be examined. Figure 4 plots the computed amplitudes of the surface function ϕ for the cases of $kd = 1$ and 5, and $N = 5$, 10 and 20. Other definitions of this figure are similar to that of Figure 2. Note that Figure 4(b) does not include the case of $N = 5$ for $kd = 5$ because the numerical result does not converge. The corresponding exact solution of the surface function can be written as [23]

$$\phi = (8\pi)^{1/2} \sum_{n=0}^{\infty} (-1)^n \left[\mathrm{i} \frac{Se_{2n}(\upsilon, 0) Se_{2n}(\upsilon, \tau)}{N_{2n}^{(e)} (\partial/\partial u) Re_{2n}^{(3)}(\upsilon, \cosh u)|_{u=0}} + \frac{So_{2n+1}(\upsilon, 0) So_{2n+1}(\upsilon, \tau)}{N_{2n+1}^{(o)} (\partial/\partial u) Ro_{2n+1}^{(3)}(\upsilon, \cosh u)|_{u=0}} \right], \tag{71}$$

where $0 \leqslant u < \infty$. Figure 4(a) indicates that the numerical result of $N = 10$ correlates well with the exact solution for $kd = 1$; the discrepancy of $N = 5$ mainly occurs at the edges. Figure 4(b) exhibits that the numerical result of $N = 20$ fits the exact solution well for $kd = 5$; the great discrepancy of $N = 10$ implies the insufficient expansion terms for the solution. Figure 5 explains the corresponding relative errors of Figure 4. The relative error of $N = 20$ is less than about 10^{-3} for $kd = 1$ and 10^{-2} for $kd = 5$, as Figure 5 shows. For $kd = 1$, doubling the expansion number from $N = 5$ to 10 improves about an order of 10^{-1} in the relative accuracy. For $kd = 5$, doubling $N = 10$ to 20 improves the relative accuracy greater than one order of 10^{-1}. Construction of the matrix elements also occupies the major

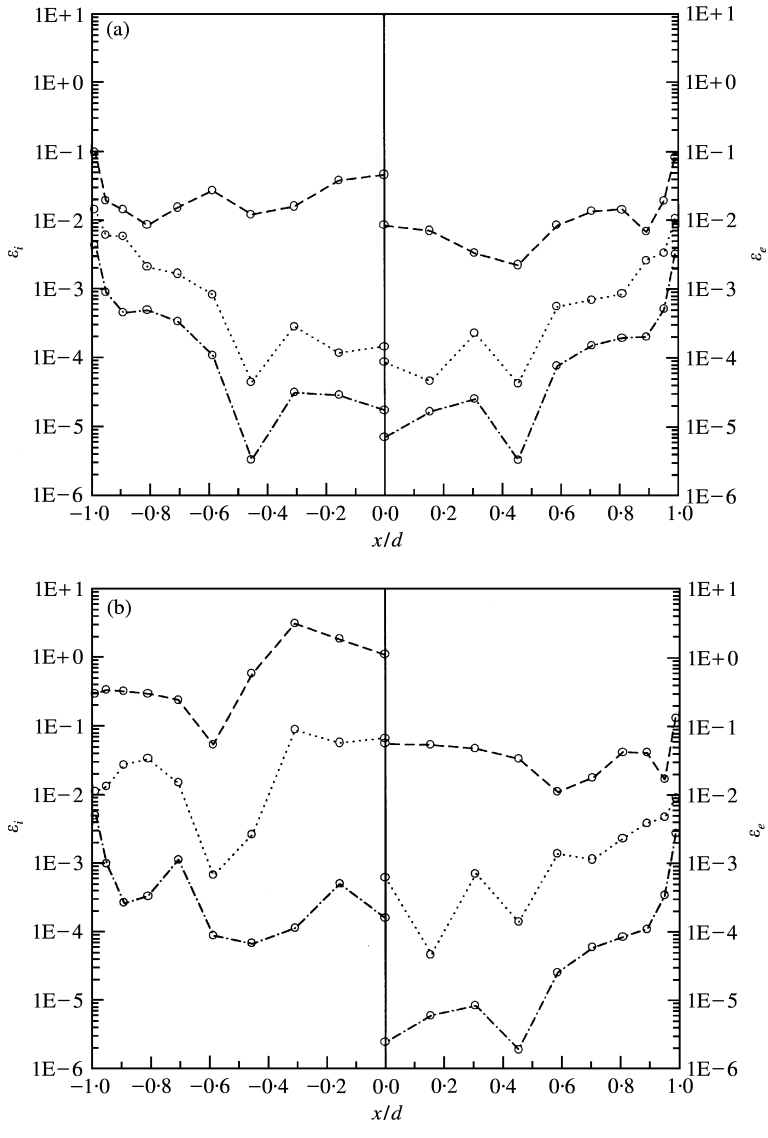

Figure 3. Relative error ε of computed amplitude of surface field in Figure 2 for (a) $kd = 1$ and (b) $kd = 5$: –·–·–·, $N = 20$; ·····, $N = 10$; – – –, $N = 5$.

portion of the computational time in this case. Figures 4 and 5 thus confirm the effectiveness of the transformed formulation presented in section 4.

In light of the above development, let us consider herein the case of the upper arch of an ellipse with major axis $2d$, minor axis $2e$, and $f^2 = d^2 - e^2$, exposed to a plane wave incident in the direction of the negative y-axis (see Figure 6). The boundary surface can be represented by $x^2/d^2 + y^2/e^2 = 1$. In this case, some related functions, e.g., the transformation function $\mathrm{d}S/\mathrm{d}\alpha$, can be evaluated analytically. However, we did not use this relation directly in the modified formulations (33) and (43) for soft bodies, and (54) and (66) for hard bodies, i.e., we treated this case as an arbitrarily shaped body with a set of given discrete surface points only. For convenience, first convert the boundary surface to $x^2 + d^2y^2/e^2 = 1$ so that $-1 \leqslant x \leqslant 1$. Forty intervals of a cubic spline were used for

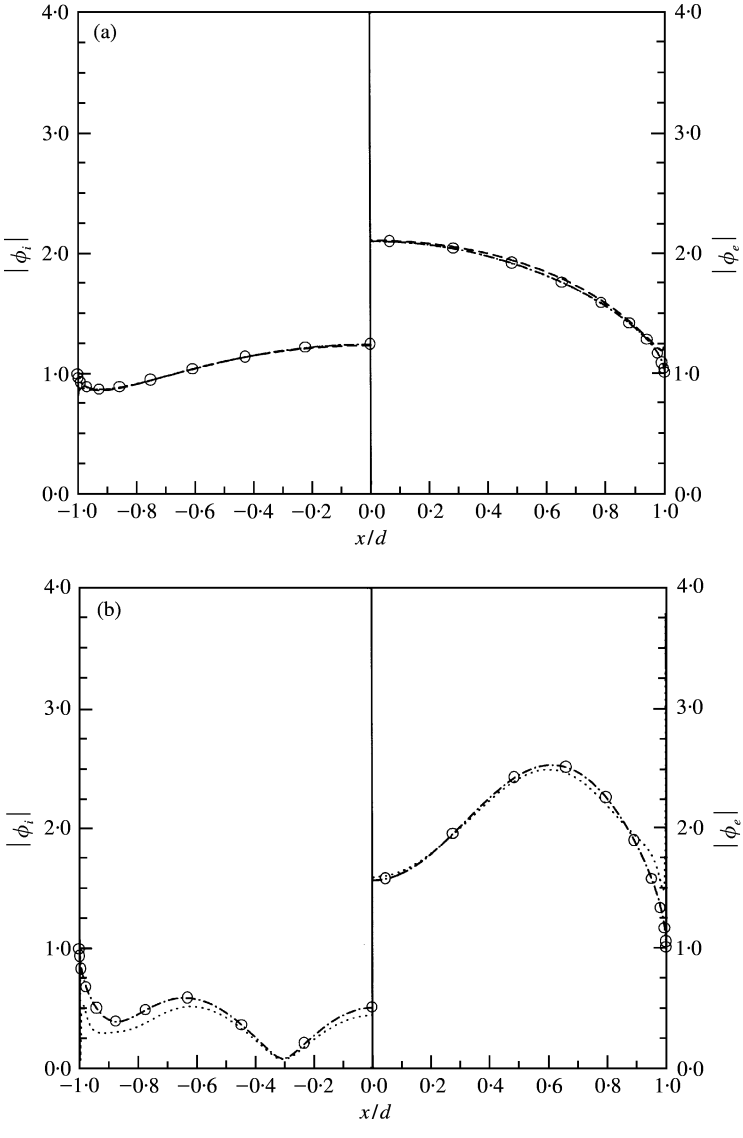

Figure 4. Amplitude of surface field for a hard flat plate exposed to a plane wave with (a) $kd = 1$ and (b) $kd = 5$: ○○○, exact solution; – · – · –, $N = 20$; · · · · ·, $N = 10$; – – –, $N = 5$.

simulating the boundary surface. In doing so, the absolute errors of $y(t)$ and $\mathrm{d}y/\mathrm{d}t$ have the values of about 10^{-7} and 10^{-6} respectively. All data of boundary points needed in the parametric formulations can then be easily obtained from the cubic spline. All calculations presented below applied the series expansion of $N = 20$. Figure 6 illustrates the variation in the surface function $|k^{-1}\partial\phi/\partial n|$ of the soft curved plate with respect to the radio e/d. One may immediately observe that the computed surface function $|k^{-1}\partial\phi_e/\partial n|$ of $e/d = 0{\cdot}5$ in Figure 6(b) approaches a value of one as $x/d \to 1$. This surface function actually reaches its minimum value 1·053 at $x/d = 0{\cdot}998$ and then tends to infinity rapidly as $x/d \to 1$, as it should be. Figure 6 indicates that the amplitude of the surface function on the shadow side approaches zero as the value of e/d increases, except in the region of $x/d \to -1$. The amplitude of the surface function on the illuminated side converges to a fixed value of two in

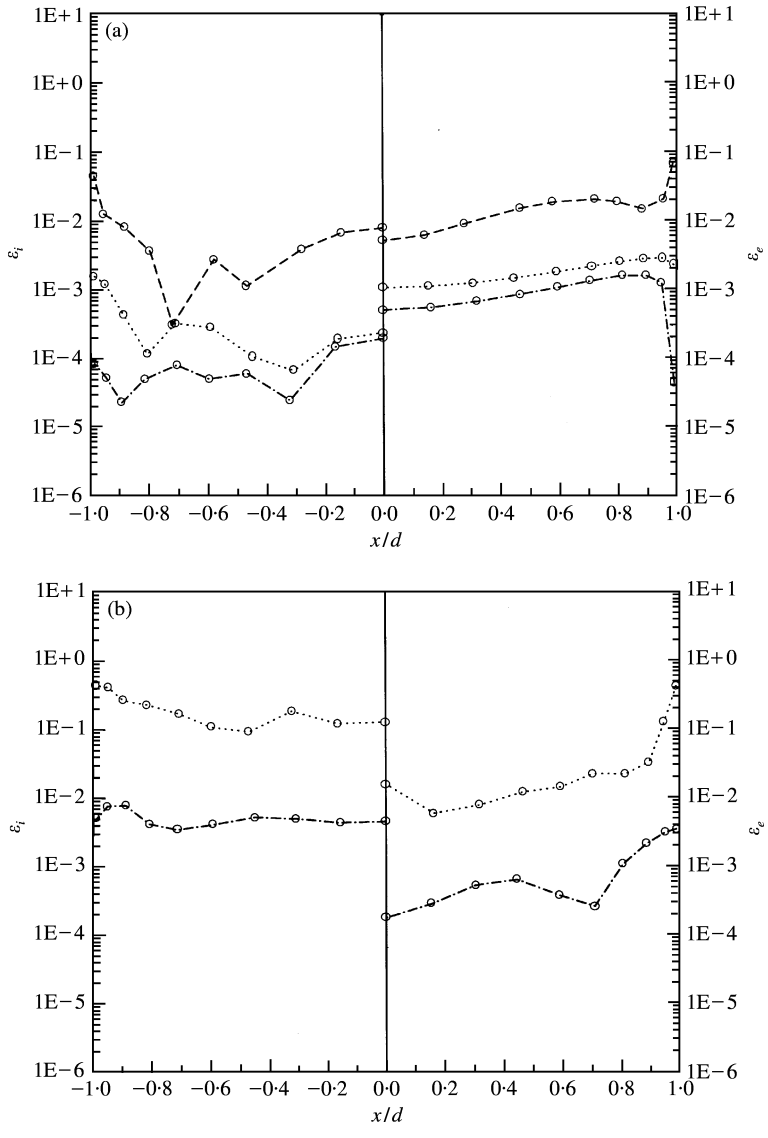

Figure 5. Relative error ε of computed amplitude of surface field in Figure 4 for (a) $kd = 1$ and (b) $kd = 5$: −·−·−·, $N = 20$; ·····, $N = 10$; − − −, $N = 5$.

the region of $x/d \to 0$ for $kf = 5$, as Figure 6(b) shows. Figure 7 illustrates the variation in the surface function $|\phi|$ of the hard curved plate with respect to the ratio e/d. The value of $|\phi_i|$ increases with an increase in the value of e/d on the shadow side for $kf = 1$, as Figure 7(a) shows; in contrast, an increase in e/d generally leads to a decrease in $|\phi_i|$ for $kf = 5$, as Figure 7(b) shows. Figures 6 and 7 have clearly demonstrated the effect of the ratio e/d on the scattering field.

6. CONCLUDING REMARKS

This paper has derived the desingularized integral formulations for investigating the acoustic scattering from 2-D thin bodies. Expansion of the unknown function into a series

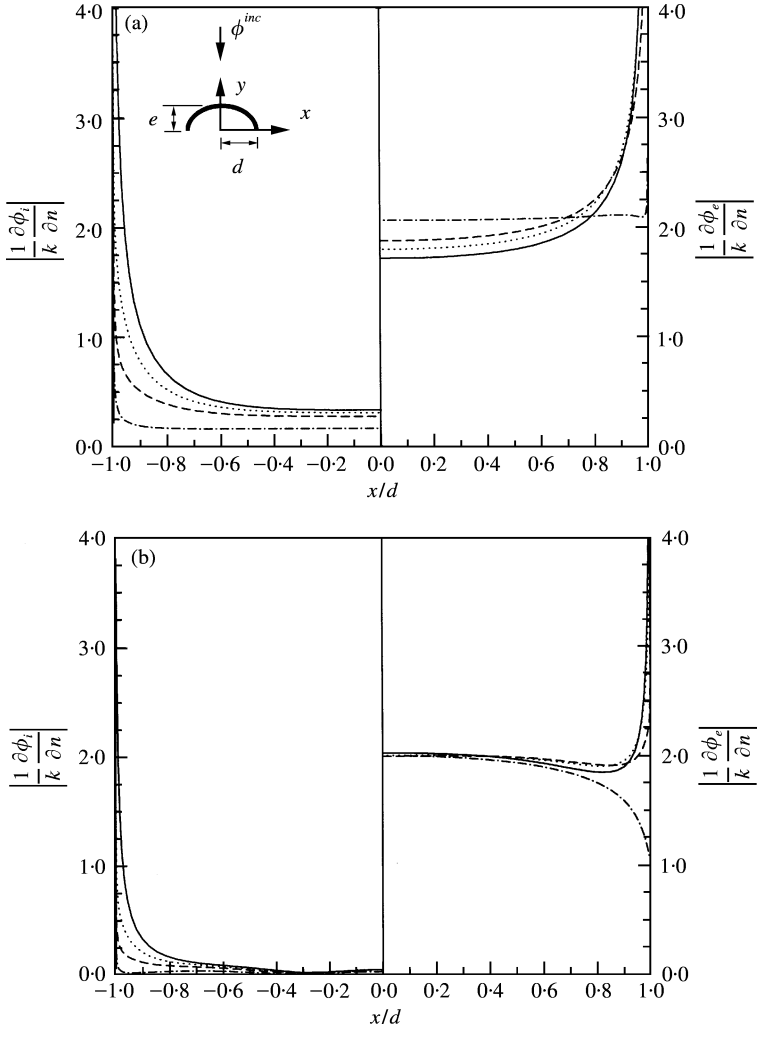

Figure 6. Amplitude of surface field for a soft curved plate exposed to a plane wave with (a) $kf = 1$ and (b) $kf = 5$, where $f^2 = d^2 - e^2$: ——, $e/d = 0$; · · · · ·, $e/d = 0{\cdot}1$; – – –, $e/d = 0{\cdot}2$; – · – · – ·, $e/d = 0{\cdot}5$.

of Chebyshev polynomials results in the direct evaluation of a number of integrals; some of them can be evaluated conveniently by applying the Gauss–Chebyshev integration rules, and others can be evaluated exactly, including the hypersingular integral. A considerable advantage of the Chebyshev expansion is that, after calculation of the series coefficients, the value of the surface function can be determined throughout the boundary surface at low computation effort, instead of at a discrete number of points occurring in the conventional boundary element methods. The proposed numerical method is applicable for arbitrarily shaped bodies because a parametric form of the boundary curve, with a cubic spline fitting, is included in the transformed formulations. The numerical implementation is highly efficient ascribed to the fact that only two basic procedures are required, i.e., one for evaluating the ordinary integrals that is straightforward, and the other for solving system of algebraic equations. Comparision of the numerical calculations with the exact solutions confirms the effectiveness of the proposed method.

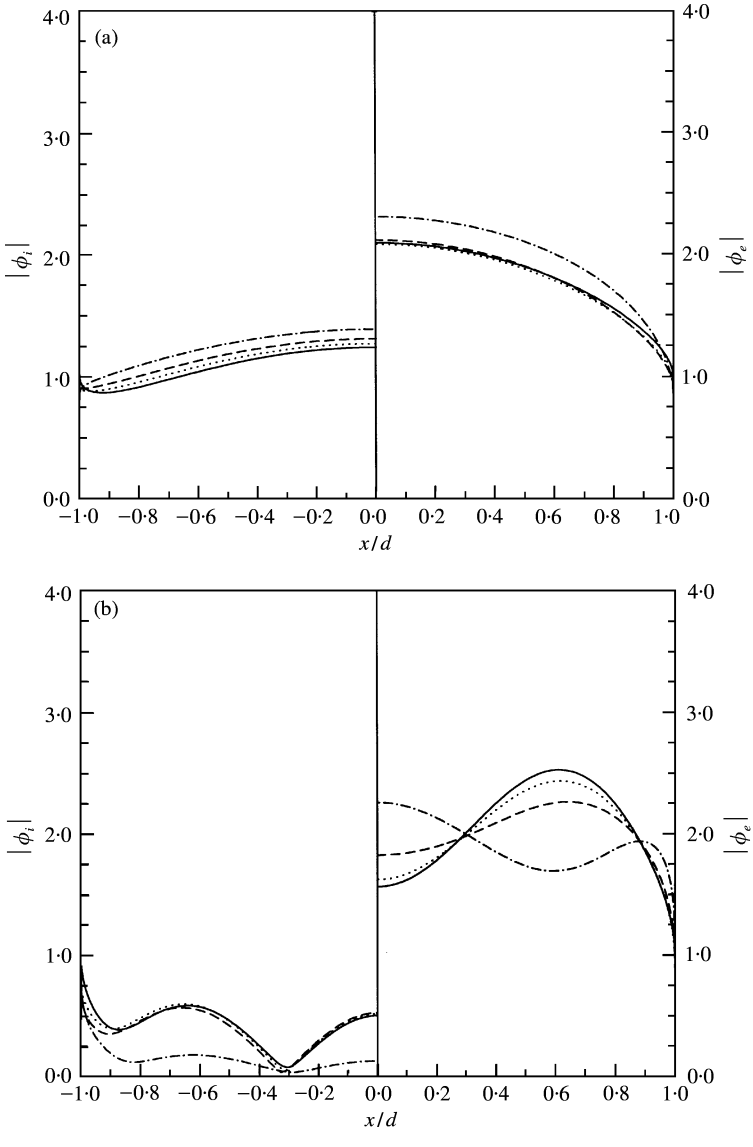

Figure 7. Amplitude of surface field for a hard curved plate exposed to a plane wave with (a) $kf = 1$ and (b) $kf = 5$: ——, $e/d = 0$; · · · · ·, $e/d = 0{\cdot}1$; – – –, $e/d = 0{\cdot}2$; – · – · –, $e/d = 0{\cdot}5$.

Also of great interest is the difference between the current approach and the conventional BEM; the comparison is summarized below.

(1) The proposed formulations are expressed in completely singularity-free form; i.e., one can immediately implement the formulations without other special treatments. The BEM approach usually involves weakly singular kernels in the integral equations before calculations and therefore necessitates further considerations for dealing with this singularity.

(2) Removing the singular behavior of the kernel at a certain point inside the integration domain by the proposed approach globally smoothes out the integration function. In

contrast, the singular kernel is only smoothed out on each element in the BEM; i.e., this approach may still possess a significantly varying integrand value over the elements that surround the singular element. This observation implies that the current approach is an accurate method for a fine discretization system.

(3) No boundary elements are required. Standard quadrature rules can be immediately applied over the entire integration domain; i.e., the collocation points can be exactly the positions at which the integration points are located. Restated, giving only nodal data (from the cubic spline fitting) is sufficient for the computation. In contrast, the BEM approach divides the boundary surface into small elements (planar or curved), and the unknown function is defined as a piecewise polynomial function. Subsequently, the application of a quadrature rule one each element yields a system of algebraic equations. Thus the number of integration points may be much more than that of elements. The above observation implies that the current element-free approach is a very efficient method.

(4) The accuracy of the surface function can be easily examined by the calculated value of the last series coefficient a_N in equation (32) (or b_N in equation (53)); i.e., if a_N is smaller than a prescribed value, say, 10^{-4}, in the first calculation, the error bound of the surface function can be approximated without a further trial. In contrast, the BEM approach generally repeats the entire numerical process at least once with different discretization systems and then compares the results for ensuring the convergence of the solution.

(5) The sought surface function can be evaluated, with the same order of accuracy, at any point on the boundary surface once the series coefficients have been determined. In other words, the accuracy is uniformly controlled. In the BEM approach, an approximation is required for evaluating surface function at a point that is not a collocation point. This also implies that the interpolation procedure may reduce the related accuracy.

Extension of the current method to 3-D thin-body scattering problems is conceptually straightforward, but it may not be an easy task. The key point lies in how to change an arbitrarily shaped thin-body into a parametric form and, meanwhile, to preserve the structure of the hypersingularity after the transformation. This extension thus necessitates an appropriate conformal mapping. For scatterers with finite volume, the Chebyshev polynomials could be replaced with other orthogonal polynomials, presuming that the corresponding analytical integration can be easily accomplished.

ACKNOWLEDGMENT

The author would like to thank the National Science Council, R.O.C., for partially supporting this research under Contract no. NSC 88-2611-E-006-008.

REFERENCES

1. P. A. Martin 1991 *Proceedings of the Royal Society London, Series A* **432**, 301–320. End-point behaviour of solutions to hypersingular integral equations.
2. A. F. Seybert, C. Y. R. Cheng and T. W. Wu 1990 *Journal of the Acoustical Society of America* **88**, 1612–1618. The solution of coupled interior/exterior acoustic problems using the boundary element method.
3. T. W. Wu and G. C. Wan 1992 *Journal of the Acoustical Society of America* **92**, 2900–2906. Numerical modeling of acoustic radiation and scattering from thin bodies using a Cauchy principal integral equation.
4. A. J. Burton and G. F. Miller 1971 *Proceedings of the Royal Society of London, Series A* **323**, 201–210. The application of integral equation methods to the numerical solution of some exterior boundary value problems.

5. H. A. SCHENCK 1968 *Journal of the Acoustical Society of America* **44**, 41–58. Improved integral formulation for acoustic radiation problems.
6. A. W. MAUE 1949 *Zeitschrift für Physik. A* **126**, 601–618. Zur Formulierung eines allgemeinen Beugungsproblems durch eine Integralgleichung.
7. W. L. MEYER, W. A. BELL, B. T. ZINN and M. P. STALLYBRASS 1978 *Journal of Sound and Vibration* **59**, 245–262. Boundary integral solutions of three-dimensional acoustic radiation problems.
8. C. C. CHIEN, H. RAJIYAH and S. N. ATLURI 1990 *Journal of the Acoustical Society of America* **88**, 918–937. An effective method for solving the hypersingular integral equations in 3-D acoustics.
9. S. A. YANG 1999 *Journal of the Acoustical Society of America* **105**, 93–105. A boundary integral equation method for two-dimensional acoustic scattering problems.
10. K.-D. IH and D.-J. LEE 1997 *Journal of Sound and Vibration* **202**, 361–373. Development of the direct boundary element method for thin bodies with general boundary conditions.
11. T. W. WU 1995 *Journal of the Acoustical Society of America* **97**, 84–91. A direct boundary element method for acoustic radiation and scattering from mixed regular and thin bodies.
12. L. FOX and I. B. PARKER 1968 *Chebyshev Polynomials in Numerical Analysis*. London: Oxford University Press.
13. D. ELLIOTT 1959–60 *Journal of the Australian Mathematical Society* **1**, 344–356. The numerical solution of integral equations using Chebyshev polynomials.
14. R. E. SCRATON 1969 *Mathematics of Computation* **23**, 837–844. The solution of integral equations in Chebyshev Series.
15. R. PIESSENS and M. BRANDERS 1976 *Journal of Computational Physics* **21**, 178–196. Numerical solution of integral equations of mathematical physics, using Chebyshev polynomials.
16. J. HADAMARD 1923 *Lectures on Cauchy's Problems in Linear Partial Differential Equations*. New Haven: Yale University Press.
17. A. C. KAYA and F. ERDOGAN 1987 *Quarterly of Applied Mathematics* **XLV**, 105–122. On the solution of integral equations with strongly singular kernels.
18. P. M. MORSE and K. U. INGARD 1968 *Theoretical Acoustics*. New York: McGraw-Hill Book Co.; Chapter 8.
19. M. ABRAMOWITZ and I. A. STEGUN (editors) 1965 *Handbook of Mathematical Functions*. New York: Dover.
20. W. H. BEYER (editor) 1991 *CRC Standard Mathematical Tables and Formulae*. Boca Raton: CRC Press.
21. V. I. SMIRNOV 1964 *A Course of Higher Mathematics*, Vol. IV. Oxford: Pergamon.
22. P. A. MARTIN and F. J. RIZZO 1989 *Proceedings of the Royal Society London. Series A* **421**, 341–355. On boundary integral equations for crack problems.
23. J. J. BOWMAN, T. B. A. SENIOR and P. L. E. USLENGHI (editors) 1987 *Electromagnetic and Acoustic Scattering by Simple Shapes*. New York: Hemisphere, Chapter 4.
24. J. A. STRATTON 1941 *Electromagnetic Theory*. New York. McGraw-Hill Book Co.; Chapter VI.